Support information

Predicting Novel 2D MB_2 (M=Ti, Hf, V, Nb, Ta) Monolayers with Ultrafast Dirac Transport Channel and Electron-orbital Controlled Negative Poisson's Ratio

Chunmei Zhang[1], Tianwei He[1], Sri Kasi Matta[1],

Ting Liao[1], Liangzhi Kou[1], Zhongfang Chen[2], Aijun Du[1,*]

[1]*School of Chemistry, Physics and Mechanical Engineering, Queensland University of Technology, Gardens Point Campus, Brisbane, QLD 4001, Australia*

[2]*Department of Chemistry, University of Puerto Rico, Rio Piedras Campus, San Juan, Puerto Rico 00931, USA*

Corresponding Author: Aijun Du, Email: aijun.du@qut.edu.au

Table S1, the optimized lattice constants a (Å) and the buckling height t (Å) for stable MB_2 monolayers (M=Be, Mg, Ti, Hf, V, Nb, Ta, Fe) and agree well with previous results.

	TiB_2	HfB_2	VB_2	NbB_2	TaB_2	BeB_2	MgB_2	FeB_2
a	3.126	3.194	3.090	2.946	2.965	3.031	3.018 (3.04[1])	3.171 (3.177[2])
t	1.196 (1.19[3])	1.417	1.076	1.681	1.631	0.582 (0.5[4])	1.686	0.632 (0.6[2])

By using searching method as implemented in the CALYPSO code, two other phases of MB_2 are also found. We name them IT and 2H. However, their energies are higher than our investigated P6/mmm structure. Table s2 give the energies comparison between three different phases, which prove that P6/mmm is the most stable phase among them.

Table S2, the energies of 1T, 2H phases relative to P6/*mmm* for explored stable MB_2 monolayers (M=Be, Mg, Ti, Hf, V, Nb, Ta, Fe)

	TiB_2	HfB_2	VB_2	NbB_2	TaB_2	BeB_2	MgB_2	FeB_2
P6mmm	0	0	0	0	0	0	0	0
1T	3.741	0.313	3.261	3.419	3.351	1.838	4.298	2.006
2H	2.018	4.605	2.538	5.049	1.29	1.844	4.882	1.985

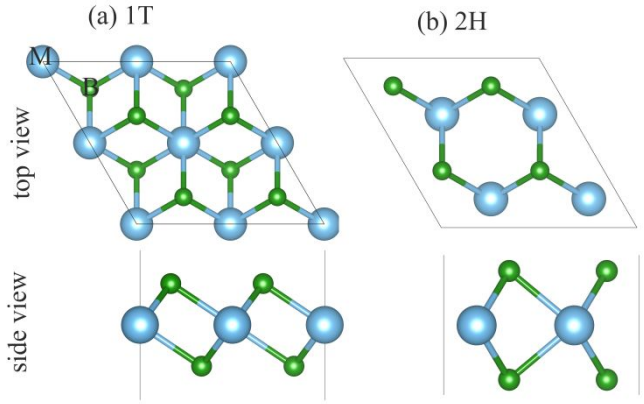

Figure S1 (a-b) 1T and 2H phases of MB_2 monolayer.

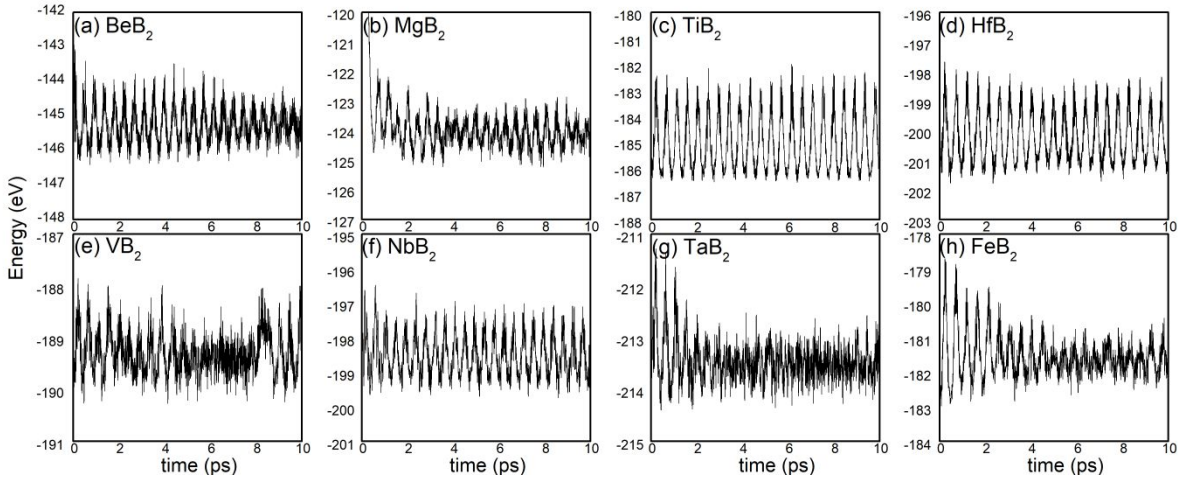

Figure S2. Ab initio MD simulations of the evolution of energy of 3x3x1 supercell monolayers MB_2 (M= Ti, Hf, V, Nb, Ta, Be, Mg, Fe) with time running for 10 ps under 700K.

Table S3, the optimized lattice constants a (Å) and the buckling height t (Å) for explored unstable MB_2 monolayers.

	CaB_2	BaB_2	ScB_2	CrB_2	MoB_2	WB_2	MnB_2	TcB_2	ReB_2
a	3.133	3.225	3.174	3.148	2.898	2.883	3.160	2.979	2.992
t	1.332	2.302	1.477	0.908	1.581	1.667	0.740	1.595	0.604
	RuB_2	OsB_2	CoB_2	RhB_2	IrB_2	NiB_2	CuB_2	AgB_2	ZnB_2
a	2.946	2.862	3.246	3.036	3.141	3.025	2.959	2.933	2.956
t	1.438	1.598	0.492	1.323	1.190	1.090	1.431	2.003	1.638
	AlB_2	GaB_2	InB_2	GeB_2	SnB_2	ZrB2			
a	2.996	2.958	3.069	3.015	2.965	3.162			
t	1.438	1.838	2.123	1.666	1.601	1.518			

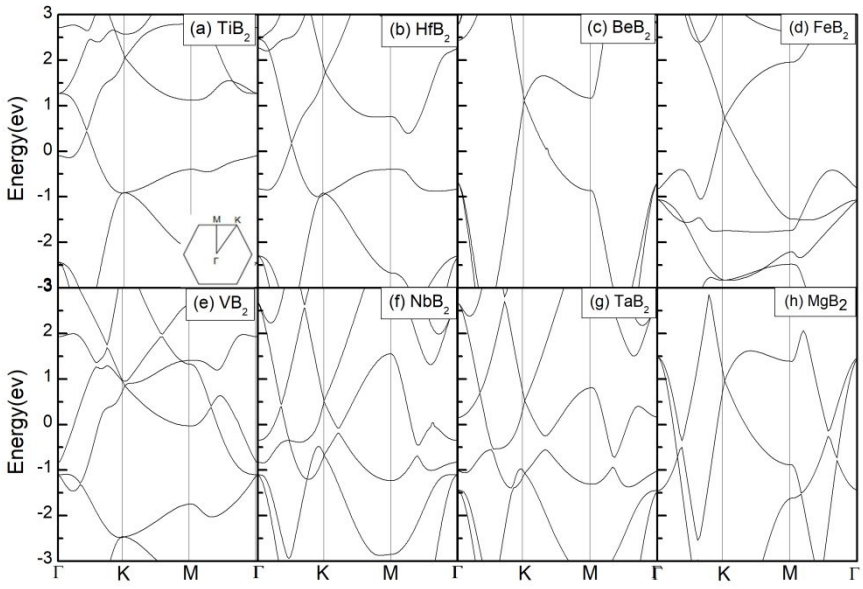

Figure S3. Band structure of MB_2 calculated by HSE method, where high-symmetry k-points are shown in the inset of (a). The Fermi level is set at the energy zero point.

Table S4 elastic constants for MB_2 monolayers.

	C11	C12	C13	C21	C22	C23
TiB_2	803.540	-33.323	3.565	-33.323	790.495	1.392
HfB_2	650.887	-127.178	6.322	-147.253	642.710	5.501
VB_2	511.014	-131.730	13.5174	-131.730	525.804	19.479
NbB_2	843.788	-19.514	5.777	-19.514	849.088	9.300
TaB_2	808.816	-64.977	9.014	-64.977	812.799	10.086
BeB_2	925.716	23.018	4.586	23.018	915.461	6.500
MgB_2	775.887	61.341	10.737	61.341	737.292	6.382
FeB_2	779.183	348.739	30.109	348.739	780.692	32.542

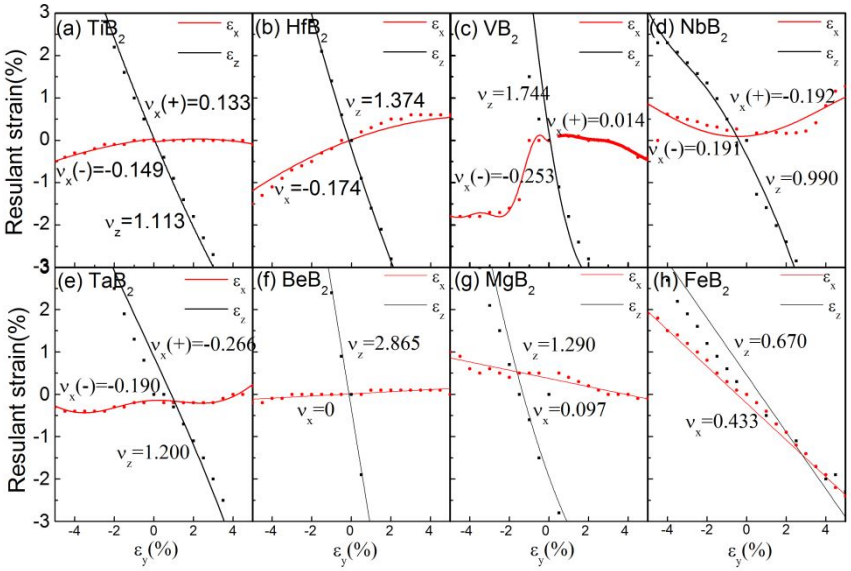

Figure S4. (a)-(h) Poisson's ratios for MB_2 (M=Ti, Hf, V, Nb, Ta, Be, Mg, Fe) as a function of strain applied along the b axis (-5%-5%). The axis x, y, and z correspond to the in-plane lateral and thickness directions, respectively.

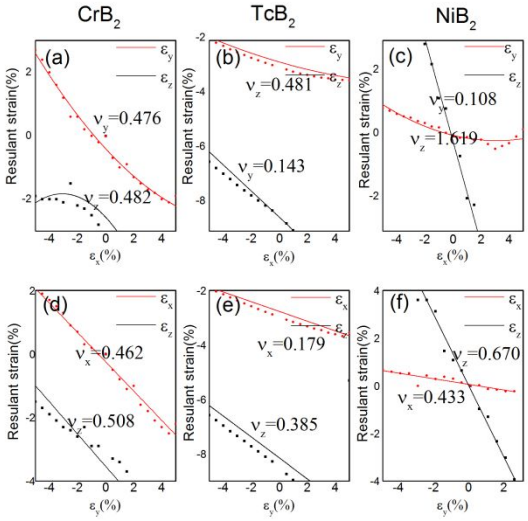

Figure S5 (a)-(f) Poisson's ratios for MB_2 (M=Cr, Tc, Ni) as a function of strain applied along a axis and b axis (-5%-5%). The axis x, y, and z correspond to the in-plane lateral and thickness directions, respectively.

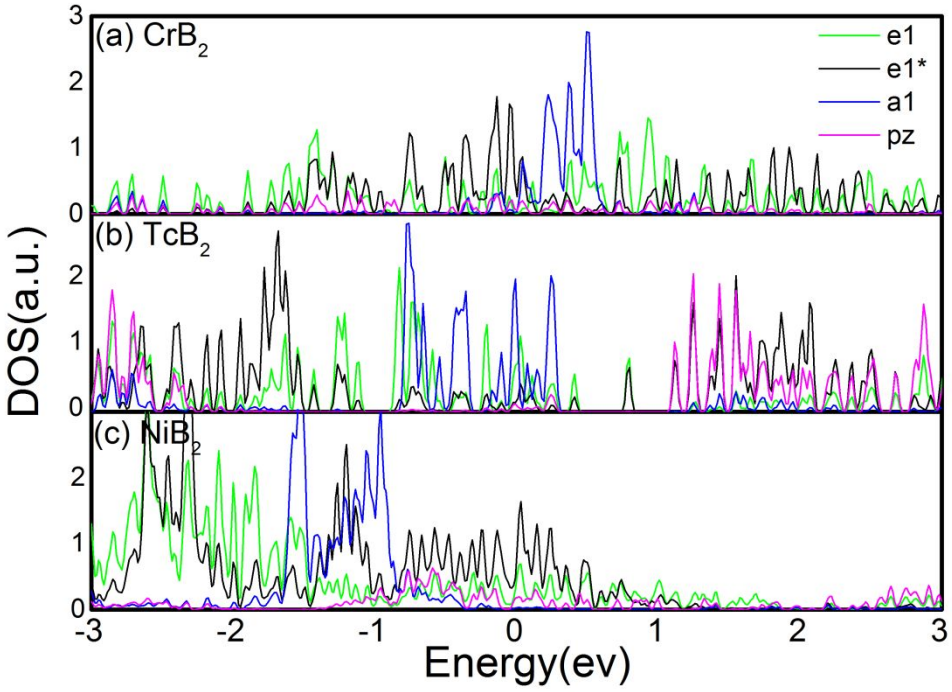

Figure S6 | DOS of MB_2. The M_d-B_p orbital coupling manifests itself in the overlap of their DOS. The DOS shown in the figure are $e1 = d_{xy} + d_{x^2-y^2}$, $e1^* = d_{xz} + d_{yz}$ and $a1 = d_{z^2}$. The Fermi level is set to 0.

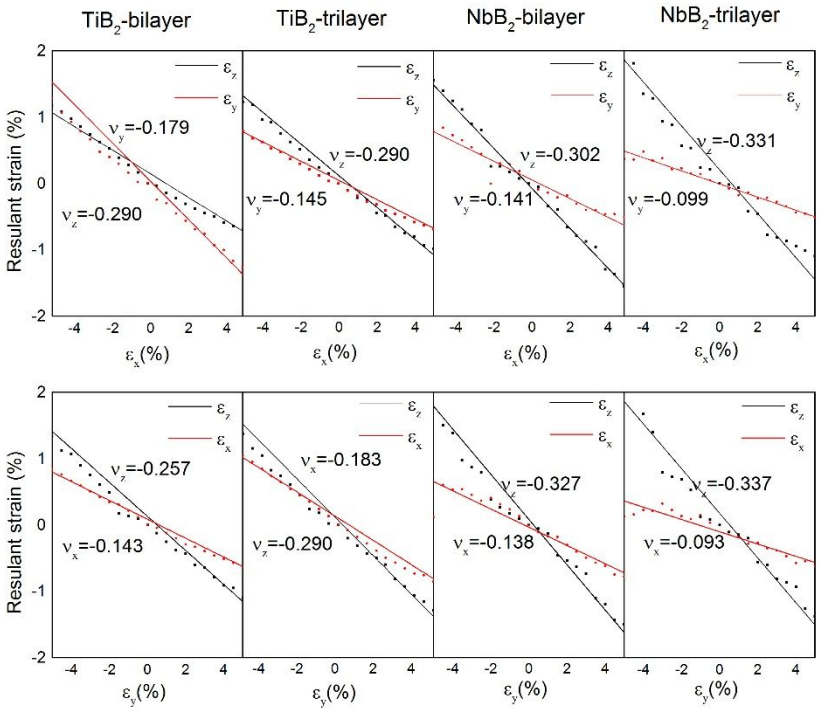

Figure S7 Poisson's ratios for bi- and tri-layer MB_2 (M=Ti, Nb) as a function of strain applied along a axis and b axis (-5%-5%). The axis x, y, and z correspond to the in-plane lateral and thickness directions, respectively.

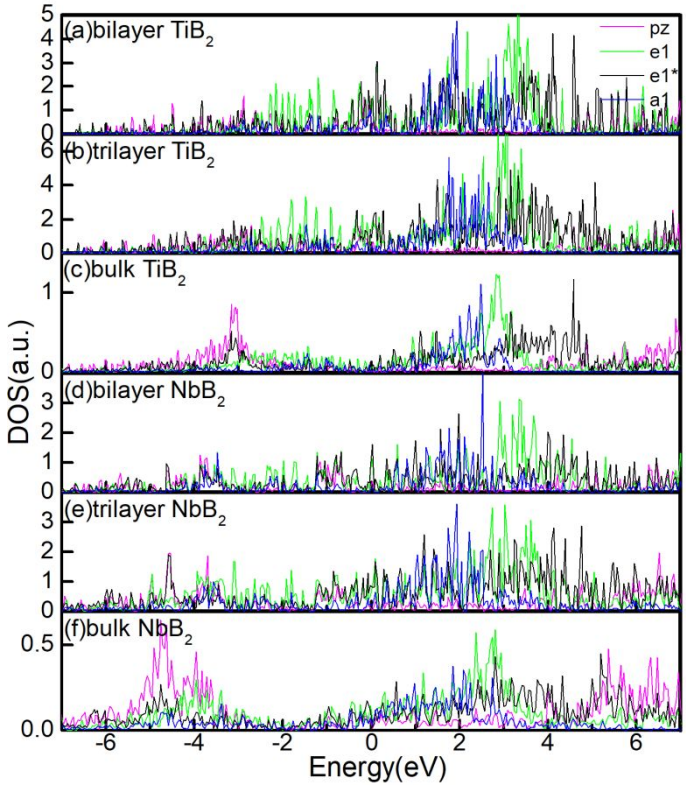

Figure S8 | DOS of bi-, tri- layer, and bulk TiB_2 and NbB_2. The M_d-B_p orbital coupling manifests itself in the overlap of their DOS. The DOS shown in the figure are $e1 = d_{xy} + d_{x^2-y^2}$, $e1^* = d_{xz} + d_{yz}$, $and\ a1 = d_{z^2}$. The Fermi level is set to 0.

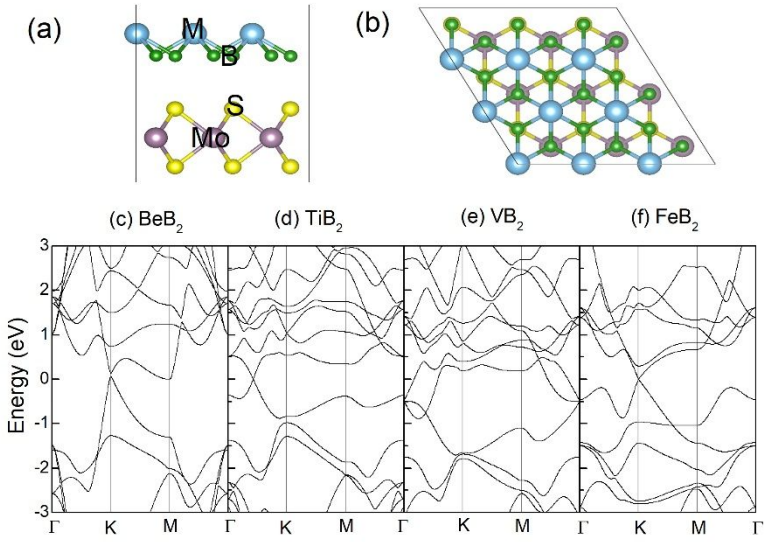

Figure S9 (a-b) the side and top views of 3x3x1 supercell of MB_2 on MoS_2 substrate. (c-f) band structure of MB_2 on MoS_2 substrate. The Fermi level is set at the energy zero point.

References

(1) Bekaert, J.; Aperis, A.; Partoens, B.; Oppeneer, P.; Milošević, M. Evolution of Multigap Superconductivity in the Atomically Thin Limit: Strain-Enhanced Three-Gap Superconductivity in Monolayer MgB_2. *Phys. Rev. B* **2017,** *96*, 094510.

(2) Zhang, H.; Li, Y.; Hou, J.; Du, A.; Chen, Z. Dirac State in the FeB_2 Monolayer with Graphene-Like Boron Sheet. *Nano lett.* **2016,** *16*, 6124-6129.

(3) Zhang, L.; Wang, Z.; Du, S.; Gao, H.-J.; Liu, F. Prediction of a Dirac State in Monolayer TiB_2. *Phys. Rev. B* **2014,** *90*, 161402.

(4) Zhang, P.; Crespi, V. H. Theory of B_2O and BeB_2 Nanotubes: New Semiconductors and Metals in One Dimension. *Phys. Rev. Lett.* **2002,** *89*, 056403.